JACS Au
AN OPEN ACCESS JOURNAL OF THE AMERICAN CHEMICAL SOCIETY

pubs.acs.org/jacsau
Article

Discovery of Spirosnuolides A−D, Type I/III Hybrid Polyketide Spiro-Macrolides for a Chemotherapeutic Lead against Lung Cancer

Thanh-Hau Huynh,[¶] Sung Chul Jang,[¶] Yeon Hee Ban, Eun-Young Lee, Taeho Kim, Ilnam Kang, Joon Soo An, Sangwook Kang, Jaeho Han, Yun Kwon, Daehyun Oh, Hyeung-geun Park, Jang-Cheon Cho, Jichan Jang, Ki-Bong Oh, Sang-Jip Nam, Sang Kook Lee,* and Dong-Chan Oh*

Cite This: *JACS Au* 2024, 4, 4821−4832

Read Online

ACCESS | Metrics & More | Article Recommendations | Supporting Information

ABSTRACT: Four new macrolides, spirosnuolides A−D (**1**−**4**, respectively), were discovered from the termite nest-derived *Kitasatospora* sp. INHA29. Spirosnuolides A−D are 18-membered macrolides sharing an embedded [6,6]-spiroketal functionality inside the macrocycle and are conjugated with structurally uncommon side chains featuring cyclopentenone, 1,4-benzoquinone, hydroxyfuroic acid, or butenolide moieties. Structure elucidation was achieved using a combination of spectroscopic analyses, multiple chemical derivatizations (methylation, methanolysis, Luche reduction, and Mosher's reaction), X-ray diffraction analysis, and computational ECD calculations. Interestingly, genome sequencing analysis suggests that spirosnuolides were biosynthesized through a rare type I/III hybrid polyketide synthase. Importantly, spirosnuolide B displayed potent antiproliferative effects against various cancer cell lines at nanomolar concentrations, particularly against HCC827 cells, an EGFR mutant non-small-cell lung cancer (NSCLC) cell line, with a high safety index value. Based on *in vitro* studies, the antiproliferative mechanism of spirosnuolide B involved the activation of AMPK signaling, leading to cell cycle arrest and apoptosis in HCC827 cells. Its potent efficacy was also proven *in vivo* by the effective inhibition of tumor growth in mouse xenograft studies. Moreover, cotreatment with spirosnuolide B and gefitinib, synergistically enhanced the antiproliferative activity and apoptosis, suggesting a potential strategy to overcome gefitinib resistance in EGFR mutant NSCLC.

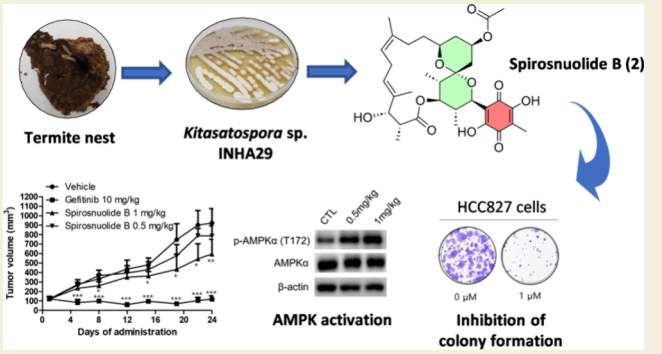

KEYWORDS: *spiroketal macrolides, type I/III polyketide synthase, lung cancer, AMPK signaling, antitumor efficacy*

INTRODUCTION

Lung cancer is the most frequently occurring cancer, with a five-year survival rate of less than 20%, constituting the highest number of cancer incidences and mortality globally.[1] Histologically, the major types of lung cancer are non-small-cell lung cancer (NSCLC) and small-cell lung cancer (SCLC). Due to the predominance of NSCLC, it has been the most extensively studied in the search for chemotherapeutic agents targeting lung cancer.[2] Current strategies for lung cancer therapy still rely heavily on chemotherapy.[3] Additionally, challenges such as undesirable side effects, nonspecific toxicity, low bioavailability, and particularly the emergence of drug resistance underscore the urgent need for novel therapeutic strategies with enhanced efficacy and reduced adverse effects.[4]

On searching for structurally interesting scaffolds, particularly those targeting cytotoxicity against lung cancer cells, we discovered four structurally novel molecules featuring both spiroketal and macrocyclic lactone motifs, named spirosnuolides A−D (**1**−**4**, Figure 1a), coupled with various side chains including cyclopentenone, dihydroxy benzoquinone, hydroxyfuroic acid, and butenolide moieties, from termite nest-derived *Kitasatospora* sp. INHA29. Structure elucidation of **1**−**4** was achieved by spectroscopic analyses (UV, IR, HRMS, and NMR), chemical derivatizations (methylation, methanolysis, Luche reduction, and Mosher's reaction), X-ray diffraction analysis, and computations. Bioinformatic analysis of the full genome of the producer strain enabled to propose that spirosnuolides A−D are biosynthesized through a rare type I/III hybrid polyketide synthase pathway. Notably, spirosnuolide B (**2**) demonstrated significant antiproliferative effects in various NSCLC cells, including HCC827 cells. Herein, we report the comprehensive structure elucidation and the biosynthetic pathway of **1**−**4** along with the *in vitro* and *in*

Received: August 31, 2024
Revised: November 27, 2024
Accepted: December 2, 2024
Published: December 10, 2024

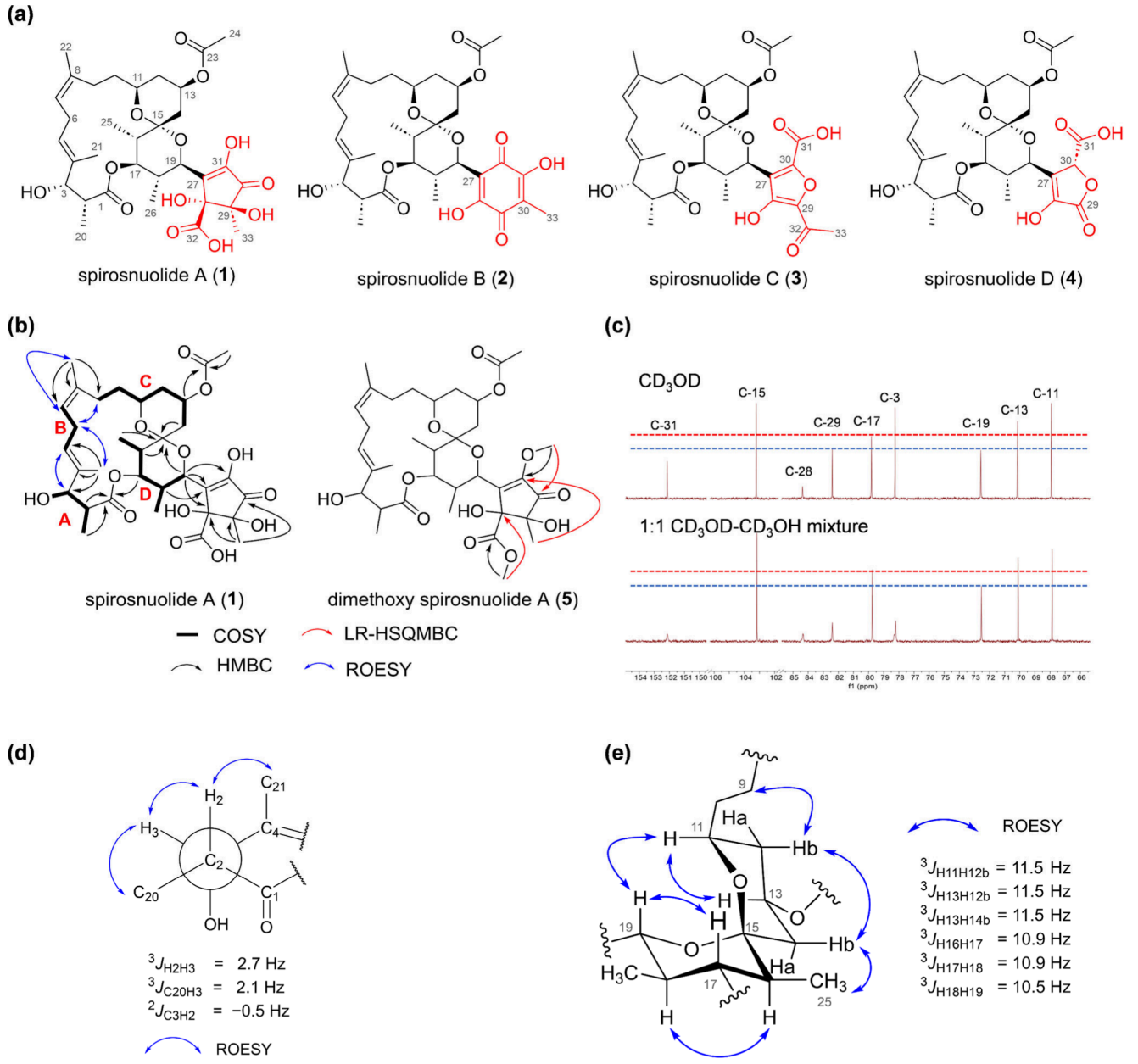

Figure 1. (a) Structures of spirosnuolides A−D (**1**−**4**, respectively). (b) Key COSY, HMBC, and LR-HSQMBC correlations for constructing the planar structure of spirosnuolide A (**1**) and its methylated derivative (**5**). (c) ^{13}C NMR spectra of spirosnuolide A (**1**) in CD_3OD (upper) and 1:1 CD_3OD-CD_3OH mixture (lower). (d) *J*-based configurational analysis for the relative configuration of spirosnuolides at C-2 and C-3. (e) Coupling constants and key ROESY correlations for determination of relative configuration of the spiro-*bis*-tetrahydropyran ketal portion of spirosnuolides.

vivo efficacy and the mechanism of action of **2** against NSCLC as a new anticancer drug lead.

RESULTS AND DISCUSSION

Structure Elucidation of Spirosnuolides

The molecular formula of spirosnuolide A (**1**) was established as $C_{33}H_{46}O_{13}$ based on high-resolution electrospray ionization mass spectrometry (HR-ESI-MS) and NMR data (Table S1), implying 11 double-bond equivalents (DBEs). Analysis of the ^{1}H, ^{13}C, and HSQC NMR spectra of **1** in CD_3OD disclosed the presence of 41 protons except five exchangeable protons and 33 carbons, along with 1-bond C−H couplings.

The ^{1}H−^{1}H COSY spectrum allowed us to identify four following spin systems: C-20−C-2−C-3 (fragment A), C-5−C-7 (fragment B), C-9−C-14 (fragment C), and C-25−C-16−C-19−C-26 (fragment D), as shown in Figure 1b. Subsequently, the allylic COSY couplings between H-5 (δ_H 5.23) and both H-3 (δ_H 3.88) and H_3-21 (δ_H 1.59), and the HMBC correlations from H_3-21 to C-3 (δ_C 78.3), C-4 (δ_C 136.9), and C-5 (δ_C 126.3) defined the connection between fragments A and B through the olefinic carbon C-4 and the attachment of the methyl group CH_3-21 to this carbon. Similarly, fragments B and C were linked through fully substituted olefinic carbon C-8 (δ_C 138.4) by the observations of an allylic COSY cross peak (H_3-22/H-7) and HMBC couplings from H_3-22 (δ_H 1.72) to C-7 (δ_C 123.9), C-8 (δ_C 138.4), and C-9 (δ_C 25.2). Key HMBC correlations from H_2-14 (δ_H 1.90/1.70) of fragment C and methyl group H_3-25 (δ_H 0.99) along with H-16 (δ_H 1.92) and H-19 (δ_H 4.55) of fragment D to quaternary carbon C-15

https://doi.org/10.1021/jacsau.4c00803
JACS Au 2024, 4, 4821−4832

Scheme 1. Chemical Derivatization of Spirosnuolide A (1)

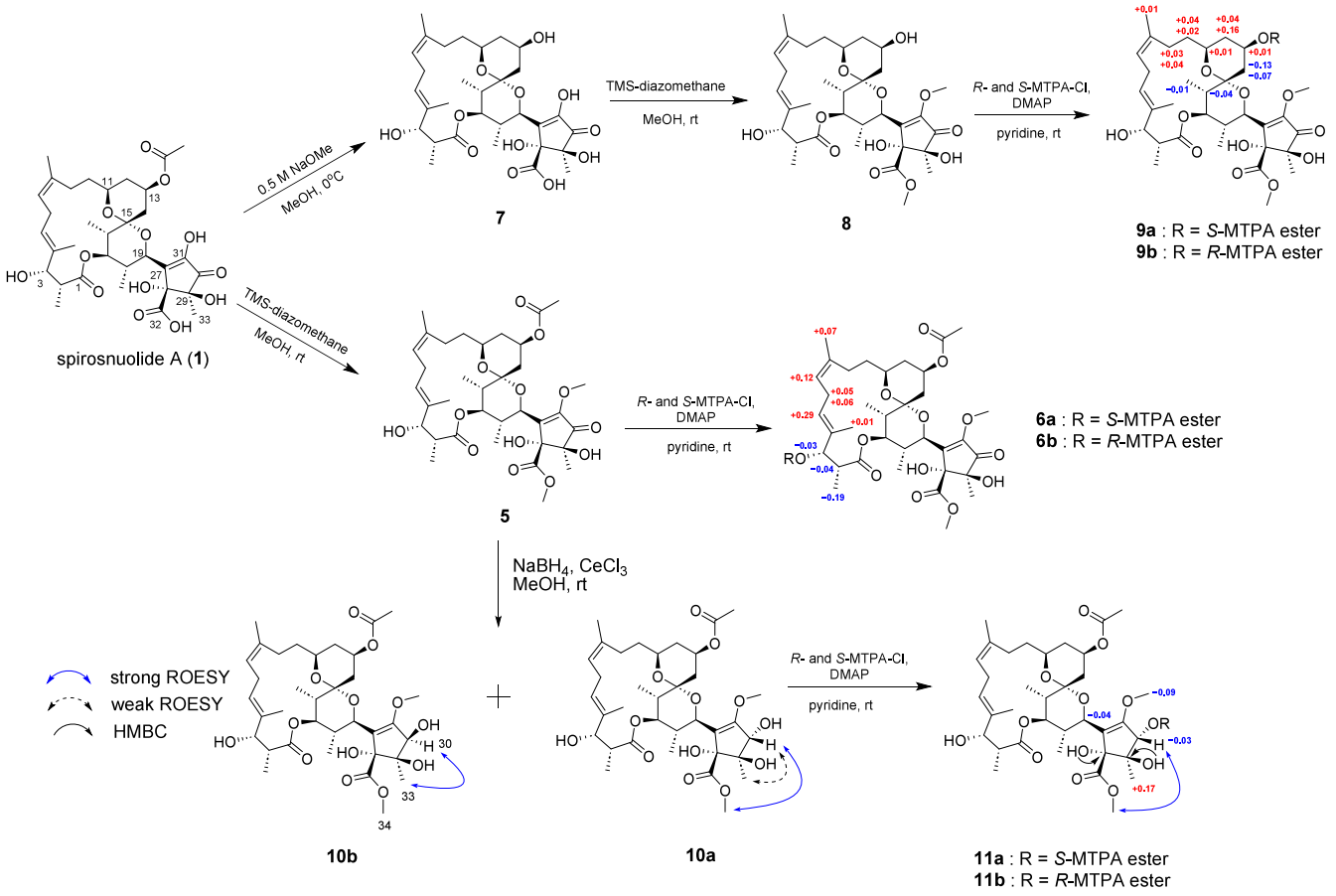

(δ_C 103.2) secured the connectivity of these fragments at C-15. Further analysis of HMBC correlations from H-2 (δ_H 2.87), H_3-20 (δ_H 1.37), and H-17 (δ_H 4.82) to carbonyl carbon C-1 (δ_C 179.6) constructed an ester bridge of fragments A and D, thus assembling the interconnection among fragments A−D to elucidate the macrocyclic lactone structure of **1**. The involvement of the hydroxy group at methine C-3 was verified by the COSY correlation (NMR data recorded in acetone-d_6) of 3-OH (δ_H 4.18) and H-3. Moreover, the attachment of an acetyl group at C-13 (δ_C 70.2) was evidently supported by the diagnostic HMBC couplings from methine H-13 and methyl H_3-24 (δ_H 2.02) to ester carbonyl carbon C-23 (δ_C 172.7).

Subsequently, the $^3J_{CH}$ and $^2J_{CH}$ HMBC cross-peaks from H-18 (δ_H 2.37) and H-19 (δ_H 4.55) to C-27 (δ_C 136.5) secured the direct linkage of C-19 (δ_C 72.6) and C-27. In addition, the conspicuous H-19/C-28 and H-19/C-31 HMBC resonances in conjunction with the strong heteronuclear correlations from singlet methyl H_3-33 (δ_H 1.32) to C-28 (δ_C 84.4), C-29 (δ_C 82.4), and C-30 (δ_C 202.3) confirmed C-31−C-27−C-28−C-29−C-30 connectivity with the methyl substitution at C-29. However, the lack of available correlations in the HMBC spectrum limited further structural analysis. To overcome this problem, **1** was derivatized with trimethylsilyldiazomethane (TMS-diazomethane) to yield the dimethoxy product **5** (Figure 1b, Scheme 1, and Table S3). In **5**, the first methylated position was placed at C-31 (δ_C 152.1) as a methoxy substitution based on the downfield carbon chemical shift of C-31 and HMBC correlation from the methoxy group 31-OCH_3 to C-31, confirming the presence of hydroxy substitution at C-31 in **1**. The other methoxy group in **5** was connected to the unassigned carbonyl carbon C-32 (δ_C 175.9) by the HMBC correlation from the methoxy protons to C-32, suggesting the presence of the free carboxylic acid 32-COOH in **1**. Furthermore, long-range heteronuclear single quantum multiple bond correlation (LR-HSQMBC), using long-range $^nJ_{CH}$ couplings (where n = 4−6),[5] enabled to observe $^4J_{CH}$ LR-HSQMBC correlation from the methyl group of the methyl ester 32-$COOCH_3$ to C-28, unambiguously assigning the carboxylic acid group 32-COOH at C-28 in **1**. Similarly, the observed LR-HSQMBC resonances from the methoxy group 31-OCH_3 to ketone carbonyl C-30 and from the methyl protons H_3-33 to C-31 constructed a cyclopentenone ring by connecting C-30 and C-31. Two quaternary carbons, C-28 (δ_C 84.4) and C-29 (δ_C 82.4), with the characteristic chemical shifts in the oxygenated carbon region, suggested their oxygen-bearing nature. Furthermore, two unobserved exchangeable protons were assigned to these two oxygenated carbons by spectroscopically analyzing the α-methoxy-α-(trifluoromethyl) phenylacetyl acid (MTPA) product **11b** (see Scheme 1 and Table S6).

The HMBC correlation from H-19 to the quaternary carbon C-15 revealed an ether bridge between C-15 and C-19 to form a tetrahydropyran ring. The above data included three carbonyl groups, two olefinic double bonds, a tetrahydropyran ring, a cyclopentenone ring, and a macrocyclic ring, accounted for ten of the 11 DBEs, thus requiring the presence of one additional ring in the structure. Therefore, the unassigned oxygen atom of oxymethine C-11 (δ_C 67.9) and the dioxygenated chemical shift for the quaternary carbon C-15 (δ_C 103.2) reasonably

https://doi.org/10.1021/jacsau.4c00803
JACS Au 2024, 4, 4821−4832

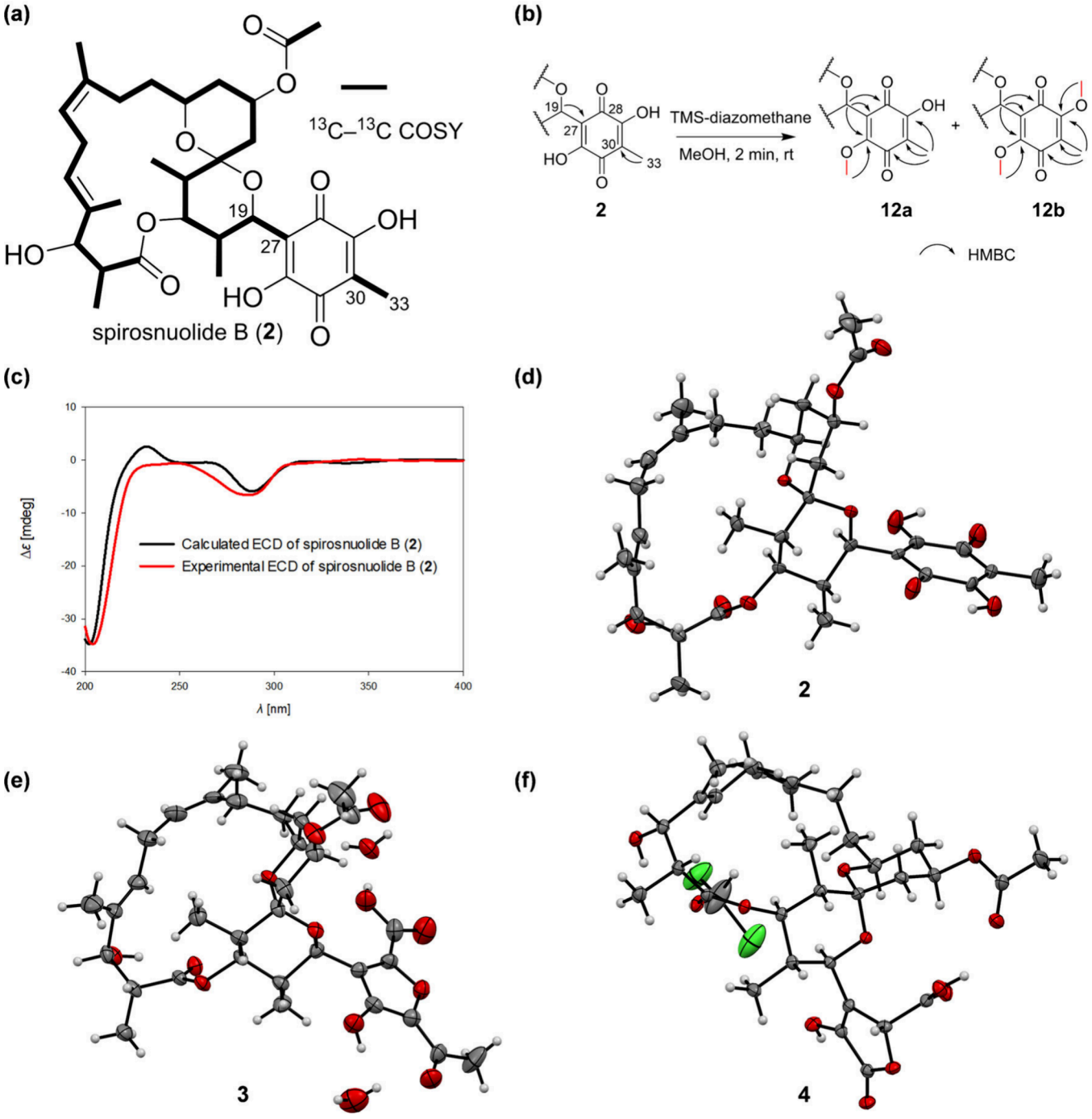

Figure 2. (a) ^{13}C–^{13}C COSY spectrum (bold line) of spirosnuolide B (**2**). (b) Methylation derivatization of spirosnuolide B with HMBC correlations (arrows). (c) Comparison of the experimental ECD spectrum with the averaged calculated ECD spectrum of spirosnuolide B (**2**). ORTEP drawings with 30% probability ellipsoids shown of the crystal structures of (d) spirosnuolide B (**2**), (e) spirosnuolide C (**3**), and (f) spirosnuolide D (**4**).

constructed the C-11−C-19 spiro-*bis*-tetrahydropyran ketal system. NMR validation of the C-11−O−C-15 linkage of this spiroketal ring remains challenging because of the absence of HMBC correlation from H-11 to C-15. To address this problem, we employed an alternative NMR technique using the β-isotope effect with deuterium incorporation experiments, of which the ^{13}C spectrum for **1** was recorded in a 1:1 mixture of CD_3OD and CD_3OH.[6,7] In this context, β-position carbinols to exchangeable protons are broadened or doubled due to the difference in energy and bond distance of hydrogen isotopes. Specifically, the carbon signals of C-3, C-28, C-29, and C-31 broadened, which was consistent with the proposed hydroxy substitutions (Figure 1c). In contrast, the carbon peaks at C-11, C-13, C-15, C-17, and C-19 were unaffected. As discussed earlier, the oxygen atoms of the carbinols C-13 and C-17 underwent acetylation and macrocyclization, respectively, and the oxygen atoms attached to C-11 and C-19 were rationally joined to C-15 to construct a bicyclic spiroketal ring. Consequently, the planar structure of **1** was defined as a

https://doi.org/10.1021/jacsau.4c00803
JACS Au 2024, 4, 4821−4832

macrolide featuring a bicyclic spiro-*bis*-tetrahydropyran ketal functionality.

Once the gross structure of **1** was elucidated, the double bond configuration for C-4/C-5 was deduced as an *E* configuration based on the ROESY correlations of H_3-21 and H_2-6, and of H-5 and H-3; whereas the C-7/C-8 double bond was assigned as a *Z* relationship based on the H-7/H_3-22 and H_2-6/H_2-9 ROESY couplings (Figure 1b). In turn, the relative configurations of the two methines, C-2 and C-3, were proposed as 2*R** and 3*S**, respectively, by applying ROESY and *J*-based configurational analysis (Figure 1d). The relative stereochemistry of the bicyclic spiroketal moiety was established as 11*S**, 13*R**, 15*R**, 16*S**, 17*R**, 18*R**, and 19*R** by analyzing the homonuclear coupling constants ($^3J_{HH}$) and ROESY correlations (Figure 1e).

To determine the absolute configuration of spirosnuolide A (**1**), a combination of chemical derivatization and spectroscopic analysis were performed (Scheme 1). Compound **5**, which has only one reactive hydroxy group at C-3, was derivatized with *R*- and *S*-α-methoxy-α-(trifluoromethyl) phenylacetyl acid (MTPA) chlorides to yield *S*- and *R*-MTPA esters (**6a** and **6b**, respectively). The distribution of positive and negative $\Delta\delta_H$ values ($\Delta\delta_H = \delta_S - \delta_R$) around C-3 allowed the determination of *S*-configuration for C-3, which subsequently assigned *R*-configuration for C-2 by the 2*R**, 3*S** relative relationship (Scheme 1). To assign the absolute configuration of C-13, the acetyl group at C-13 was cleaved by methanolysis to produce deacetyl spirosnuolide A (**7**), which possesses a secondary hydroxy group at C-13. Subsequently, **7** was methylated to yield **8** by treatment with TMS-diazomethane, and then *R*- and *S*-MTPA-Cl esterification of **8** yielded *S*- and *R*-MTPA esters (**9a** and **9b**). Comparing the signs of $\Delta\delta_{S-R}$ values established the absolute configuration of C-13 to be *R*. Referring to the earlier proposed stereochemistry analysis, the absolute configuration of the other stereogenic centers of the spiroketal ring was then assigned as 11*S*,13*R*,15*R*,16*S*,17*R*,18*R*,19*R*.

The stereochemically undetermined stereogenic centers C-28 and C-29 on the cyclopentenone ring require additional chemical modifications to assign their configurations. First, the ketone at C-30 in **5** is reduced to yield two alcoholic products (**10a** and **10b**) (Scheme 1). In **10b**, a significant ROESY correlation was observed between H-30 and H_3-33, but not with 32-$COOCH_3$, suggesting that H-30 and the methyl group CH_3-33 were on the same side of the five-membered ring, whereas the methoxycarbonyl group of 32-$COOCH_3$ was on the other side. In contrast, in **10a**, H-30 and 32-$COOCH_3$ were on the same side but were oppositely orientated to the methyl group CH_3-33 based on a very weak ROESY correlation between H-30 and H_3-33 and a strong correlation between 32-$COOCH_3$ and H-30. This result indicates that the two hydroxy groups at C-28 and C-29 in **1** have an *anti*-relationship. Compound **10a** was subjected to Mosher esterification to give two MTPA esters, **11a** and **11b** (Scheme 1). The analysis of $\Delta\delta_{S-R}$ values revealed 30*R* configuration in **10a**, thus assigning 28*R* and 29*S* configurations. The absolute configuration of the stereogenic centers in **1** was fully established to be 11*S*,13*R*,15*R*,16*S*,17*R*,18*R*,19*R*,28*R*,29*S*.

Spirosnuolide B (**2**) was purified as block-like crystals with the molecular formula $C_{33}H_{44}O_{11}$, agreeing with the HR-ESI-MS data ($[M + Na]^+$ *m*/*z* 639.2758, calculated 639.2776). However, only 29 carbon peaks were observed in the ^{13}C NMR experiments, even in various NMR solvents (CD_3OD, DMSO-d_6, and $CDCl_3$), compared with the presence of 33 carbon atoms in the molecular formula determined by HR-ESI-MS (Table S1). Twenty-six of these 29 carbon signals and their corresponding proton signals in the 1D NMR spectra were identical to those of the C-1−C-19 macrolactone backbone in **1**, indicating a structural similarity. Further detailed analysis of HSQC, COSY, and HMBC spectra of **2** confirmed the C-1−C-19 cyclic macrolactone incorporating the spiro-*bis*-tetrahydropyran ketal moiety.

The three unassigned carbons and protons observed in the NMR spectra comprised a singlet methyl group (δ_C/δ_H 7.5/1.87) and two nonprotonated sp^2 carbons (δ_C 113.7 and 113.0). C-27 (δ_C 113.0) was connected to C-19 in the above-defined macrolide structure by H-18/C-27 and H-19/C-27 HMBC correlations. The singlet methyl group CH_3-33 and the last nonprotonated sp^2 carbon C-30 (δ_C 113.7) were coupled in the HMBC spectrum but did not correlate with the elucidated partial structure.

The assembled macrocyclic structure with a spiroketal moiety accounted for seven out of 12 degrees of unsaturation, as calculated from the molecular formula. Therefore, the final partial structure must contain five double-bond equivalents. The UV spectrum of **2** showed a maximum absorption wavelength of 288 nm. These suggested that the missing moiety, constructed with $C_7H_5O_4$, including the unassigned three detected carbons (δ_C 113.7, 113.0, and 7.5) and four undetected carbons, most likely bears a long-wavelength UV chromophore because the macrocyclic structure does not possess a conjugated double bond. This proposed moiety was consistent with the MS/MS fragment ($C_7H_6O_4Na$ *m*/*z* 177.0150, calculated as 177.0158) found in the HR-ESI-MS-MS spectrum (Figure S133). Our efforts to record 2D $^{13}C-^{13}C$ COSY NMR spectra (Figure S44) and acquire 1D ^{13}C spectra at a higher temperature (DMSO-d_6, 363 K) were unsuccessful in obtaining undetectable NMR signals for hydrogen and carbon. However, the $^{13}C-^{13}C$ COSY spectrum reinforced the aforementioned structure of the macrolide backbone, as shown in Figure 2a. To introduce more protons, possibly providing more HMBC correlations to the unidentified partial structure, we derivatized **2** with TMS-diazomethane and obtained the mono- and dimethoxy products of **2** (**12a** and **12b**, respectively). Fortunately, four more carbons (two carbons at ∼160 ppm and two carbons at ∼185 ppm) were detected in the NMR spectra of **12a** and **12b**, which facilitated the structures of **12a** and **12b** as mono- and dimethoxy 1,4-benzoquinone-bearing spiro macrocyclic lactones based on the observed HMBC correlations shown in Figure 2b. The inability to detect the four oxygenated carbons within the benzoquinone moiety of **2** has been previously documented, attributed to tautomeric interconversion between two energetically equivalent forms of 2,5-dialkyl-3,6-dihydroxy-1,4-benzoquinones.[8] This tautomeric phenomenon has been reported in a few natural products (maesaquinone,[9] embelins,[10] and cinnamomycin A[11]) and synthetic compounds.[12] Therefore, the structure of spirosnuolide B (**2**) was deduced as a new macrocyclic lactone possessing a methyl dihydroxy 1,4-benzoquinone. The structure and its configuration were unequivocally supported by ECD calculations and X-ray crystallography (Figures 2c and 2d, respectively).

HR-ESI-MS measurement established a molecular formula for spirosnuolide C (**3**) ($C_{33}H_{44}O_{12}$, $[M + Na]^+$ *m*/*z* 655.2706, calculated 655.2725). An extensive examination of the 1D and 2D NMR spectra (Table S1) suggested the structural similarity

https://doi.org/10.1021/jacsau.4c00803
JACS Au 2024, 4, 4821−4832

to those for **1** and **2** on the C-1−C-19 spiroketal macrolactone backbone, and the main difference was attributed to the side chain. The full structure assignment was obscured due to the absence of HMBC correlations in the side chain. Alternatively, NMR spectra of the methylation product of **3** (**13**, Table S7) was analyzed to construct the structure of the 5-acetyl-4-hydroxy-2-furoic acid moiety (Figure 1a). Suitable crystals of **3** for X-ray crystallographic analysis confirmed the assignment (Figure 2e).

Spirosnuolide D (**4**) was isolated as white block-like crystals with a molecular formula ($C_{31}H_{42}O_{12}$). Comparison of its NMR data with **1**−**3** and subsequent analysis of 2D NMR spectra elucidated the side chain as 2-hydroxy-2-butenolide-4-carboxylic acid (Figure 1a). Single-crystal X-ray diffraction provided definitive evidence of the elucidated planar structure of **4** and also allowed the unambiguous assignment of its absolute configuration (Figure 2f).

Identification of Biosynthetic Gene Cluster of Spirosnuolides

The bioinformatics analysis of the whole genome of *Kitasatospora* sp. INHA29 with antiSMASH 7.0[13] revealed 48 biosynthetic gene clusters (BGCs), only one of which was identified as a putative modular PKS-encoded candidate for spirosnuolide biosynthesis using a retrobiosynthetic approach (Table S8 and Figure S1). Briefly, the putative spirosnuolide BGC contained five type I polyketide synthases (PKSs) (SpiA−SpiE) encoding ten modules and one type III PKS (SpiP), suggesting that spirosnuolides are assembled by a hybrid type I/III PKS system.

The type III PKS along with a series of tailoring enzymes is responsible for the biosynthesis of the starter unit 3,5-dihydroxybenzoic acid (3,5-DHBA), leading to the unusual moieties like cyclopentenone, 1,4-benzoquinone, hydroxyfuroic acid and butenolide in spirosnuolides A−D. Homology-based BGC analysis revealed that the six-gene cassette (*spiK*−*spiP*) found in the *spi* cluster shares high sequence similarity (50−71% identity) with genes encoding the starter unit 3,5-DHBA in the biosynthesis of the kendomycins[14,15] and cinnamomycins.[11] It was natural to expect that the formation of 3,5-DHBA from malonyl-CoA would be sequentially catalyzed by SpiK−SpiP (Figure S1 and Table S9).

Although the biosynthetic pathways of spirosnuolides and kendomycin differ fundamentally, the structural similarity in PKS architecture suggests that the acyl-CoA ligase domain located in the loading module of SpiA is responsible for activating the 3,5-DHBA starter unit and attaching it to the acyl carrier protein domain.[15] Additionally, it can be anticipated that the adjacent five modular PKSs (SpiA−SpiE) comprising nine extension modules will assemble the linearized polyketide skeleton of spirosnuolides. With respect to defining the biosynthetic origin of spirosnuolides, we conducted genome analysis to compare the gene-derived absolute configuration with those defined based on the chemical derivatizations and spectroscopic analyses (Figure S2). The genetic analysis-based predictions completely agreed with the stereochemistry determined by chemical methods.

After the primary chain is completed, there is a possibility that the spiroketal ring is formed spontaneously before being released by the thioesterase domain for macrocyclization. Another scenario involves using unknown enzymes similar to AveC- or RevJ-like proteins, in spiroketal formation.[16,17] However, gene products expected to be involved in spiroketal formation were not found in the *spi* gene cluster, indicating the possibility of alternative enzymes outside the biosynthetic cluster. Since these spirocyclases are mechanistically similar but phylogenetically distinct, identifying candidates may not be easily achieved through homology comparisons at the sequence level.[18]

Various post-PKS tailoring steps are expected to occur after the polyketide chain is released. A five-gene cassette (*spiF*−*spiJ*) is located immediately downstream of the PKS genes, which may account for the polyketide modifications that produce spirosnuolide B (**2**) (Figure S1). Regarding the biosynthesis of other spirosnuolides, it has been reported that a microbial transformation strain, *Actinoplanacete* sp. ATCC 53771 was capable of converting a 2,5-dihydroxy-3,6-*bis*-indolyl-1,4-benzoquinone structure known as demethylasterriquinone (DMAQ) B1, extracted from tropical fungus (*Pseudomassaria* sp.), to a *bis*-indolyl-hydroxyfuroic acid.[19] We conceive that a ring contraction of 1,4-benzoquinone moiety would occur via an enzymatic process and further ring rearrangements to convert **2** to the other spirosnuolides (Figure S1).

Antiproliferative Activities of Spirosnuolides in Human NSCLC Cancer Cells

To evaluate the biological activity of the spirosnuolides, these compounds were subjected to various bioassays including antibacterial, antifungal, and antiproliferative tests (see Supporting Information for details). The antimicrobial assay revealed that spirosnuolides A, B, and D displayed only weak antibacterial activity (Table S10). However, in their antiproliferative effect evaluation on human cell lines, spirosnuolide B (**2**) strongly inhibited the growth of various human solid cancer cells, with IC_{50} values ranging from 0.016−1.78 μM (Table S12). Compared to the lung cancer cell line (A549), the growth inhibitory activity of **2** against the lung epithelial normal cell line (MRC-5) was relatively low, suggesting selective growth inhibition in cancer cells compared to normal cells. Because **2** effectively inhibited the growth of A549 non-small-cell lung cancer cells (NSCLC), we evaluated the growth of NSCLC cell lines. As shown in Table S13, spirosnuolide B (**2**) effectively inhibited the growth of various human lung cancer cells, with IC_{50} values ranging from 0.018−0.114 μM. **2** also exhibited a high safety index (SI) value (IC_{50} value in cancer cells/IC_{50} value in normal lung epithelial MRC-5 cells) ranging from 27.3−172.8. The HCC827 cell line, which is an EGFR mutant cell line sensitive to gefitinib, was selected for further elucidation of the antiproliferative activity and plausible molecular mechanism of action of **2** in cancer cells. **2** exhibited effective antiproliferative activity in a time- and concentration-dependent manner in HCC827 cells (Figure 3a). **2** also suppressed colony formation in HCC827 cells (Figure 3b).

AMPK, a 5′ AMP-activated protein kinase, acts as a primary regulator of cellular energy homeostasis and is activated by various metabolic stresses.[20] In cancer cells, however, the activation of AMPK is considered to be associated with tumor suppressive[21] and thus is a potential candidate for cancer therapeutics.[22] In particular, several studies have shown that activation of AMPK inhibits the growth and survival of lung cancer cells, promotes cell cycle arrest and apoptosis,[23−26] and enhances the sensitivity of EGFR-targeted chemotherapies.[27−29] On this line, the effects of spirosnuolide B (**2**) on the expression of phosphorylated AMPKα (activated form)

https://doi.org/10.1021/jacsau.4c00803
JACS Au 2024, 4, 4821−4832

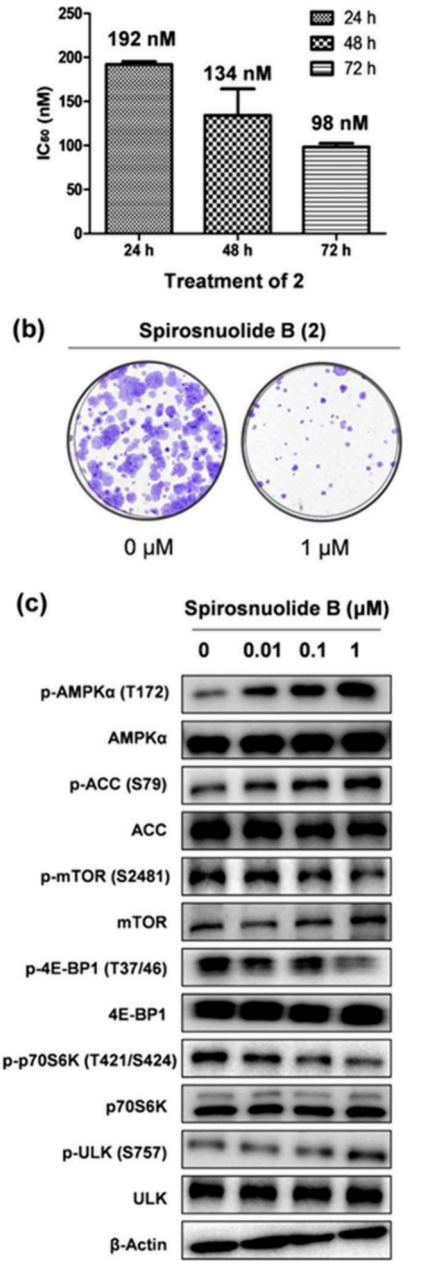

Figure 3. *In vitro* efficacy of spirosnuolide B (**2**). (a) HCC827 cells were seeded in 96-well plates and treated with spirosnuolide B (**2**) for 24−72 h. IC_{50} values were determined by SRB assay. Data are presented as mean ± SD (n = 3). (b) Effects of spirosnuolide B (**2**) on colony formation in HCC827 cells. HCC827 cells were treated with 1 μM spirosnuolide B (**2**) for 24 h, and then cells were replaced with fresh medium every 3 days and incubated for additional 21 days. (c) HCC827 cells were treated with indicated concentrations of spirosnuolide B (**2**) for 24 h, and the expression of AMPKα and its downstream targets was evaluated by Western blot analysis. β-Actin was used as an internal control.

and its downstream signals were determined in HCC827 cells. Spirosnuolide B (**2**) effectively enhanced the expressions of phosphorylated AMPKα and its downstream targets, phosphorylated ACC[30] and ULK,[31] but the expressions of phosphorylated mTOR1, 4E-BP-1, and p70S6K[32] were downregulated in HCC827 cells (Figure 3c).

Since AMPKα is also known to be associated with regulating the cell cycle in cancer cells, the effect of spirosnuolide B (**2**) on the cell cycle regulation was analyzed. The cell populations in the G_0/G_1 phase were increased from 51.8% (control group) to 65.5% (2 μM spirosnuolide B) in a concentration-dependent manner in HCC827 cells (Figures 4a and S13).

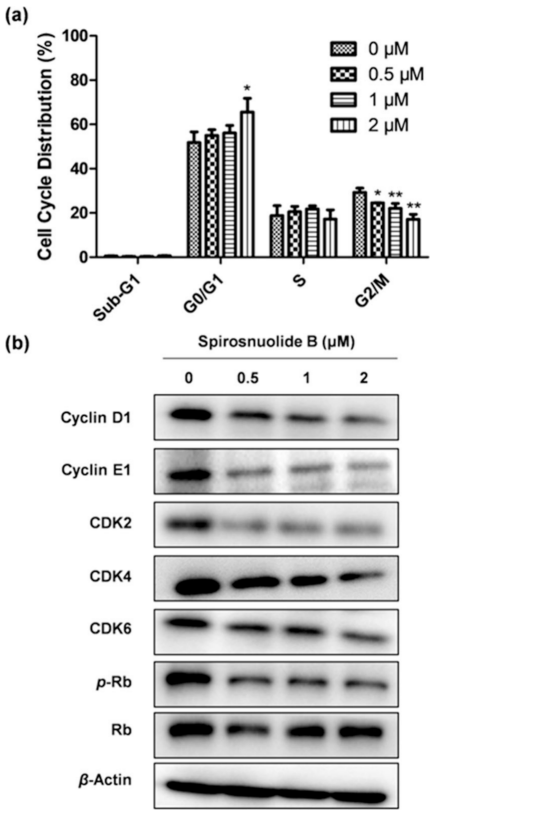

Figure 4. Effects of spirosnuolide B (**2**) on cell cycle distribution in HCC827 cells. (a) Cells were treated with spirosnuolide B (**2**) for 24 h, and then the cells were collected, fixed with 70% cold ethanol in PBS, and stained with propidium iodide (PI). Cell cycle distribution was measured by flow cytometry. *p < 0.05 and **p < 0.01 represent statistically significant differences compared to the vehicle-treated control group. (b) Cells were treated with indicated concentrations of spirosnuolide B (**2**) for 24 h, and then the expressions of proteins were analyzed by Western blotting. β-Actin was used as an internal control.

Spirosnuolide B (**2**) also effectively suppressed the expression of CDK4/6-cyclin D1, CDK2-cyclin E1, and phosphorylated Rb,[33,34] which are critical in G_0/G_1 cell cycle arrest[35] (Figure 4b).

As the activation of AMPK is also associated with the induction of apoptosis, further studies were performed to evaluate whether spirosnuolide B (**2**) could induce apoptosis in HCC827 cells. As shown in Figures 5a and S14, the early apoptotic cell populations were significantly increased with the treatment of 5 μM or 10 μM spirosnuolide B (**2**). The induction of apoptosis was further confirmed by the expression of apoptosis-associated biomarker proteins, including the upregulated expression of cleaved caspase-8, cleaved caspase-9, and cleaved PARP, and the downregulation of Bcl-xL expression in HCC827 cells (Figure 5b).

Antitumor Activity of Spirosnuolide B (2) in Nude Mouse Xenograft Models

To determine the *in vivo* efficacy of spirosnuolide B (**2**), the HCC827 cell-implanted nude mouse model was conducted. As

https://doi.org/10.1021/jacsau.4c00803
JACS Au 2024, 4, 4821−4832

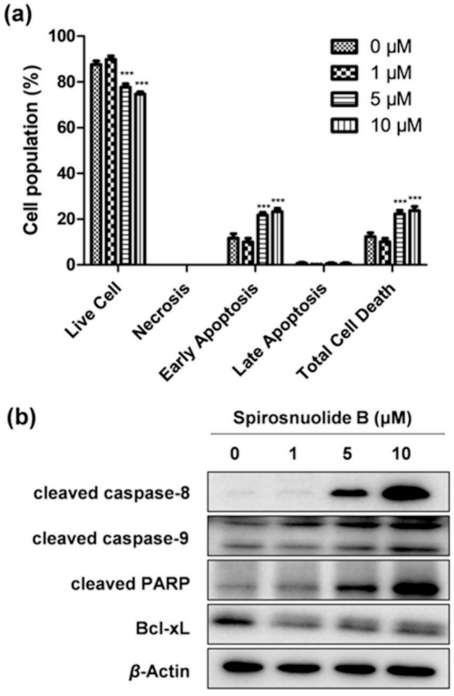

Figure 5. Effects of spirosnuolide B (**2**) on induction of apoptosis in HCC827 cells. (a) Cells were treated with spirosnuolide B (**2**) for 48 h, collected, stained with PI, and annexin V-FITC for 15 min, and apoptotic cell distribution was analyzed by flow cytometry. ***p < 0.001 represents a statistically significant difference compared to the vehicle-treated control group. (b) Cells were treated with spirosnuolide B (**2**) for 48 h, lysed, and then expressions of proteins were determined by Western blot analysis. β-Actin was used as an internal control.

shown in Figure 6a, spirosnuolide B effectively inhibited tumor growth, with tumor inhibition of 14.8% and 35.4% in the 0.5 and 1 mg/kg spirosnuolide B-treated groups, respectively, compared to the control group. No significant changes in body weight or toxicity were observed in the spirosnuolide B-treated groups (Figure 6b). Consistent with the *in vitro* findings, the immunohistochemical analysis of tumor tissue showed a decrease in a proliferation biomarker K_i-67 and an increase in the expression of p-AMPKα (T172) (Figures 6c and S15).

Combination Effects of Gefitinib and Spirosnuolide B (2) on Antiproliferation in HCC827 Cells

Gefitinib, an epidermal growth factor receptor-tyrosine kinase inhibitor (EGFR-TKI), is commonly used to treat patients with NSCLC. However, its long-term effectiveness is uncertain due to the development of acquired resistance. Hence, finding an efficient drug combination with gefitinib to overcome the acquired resistance is crucial.[36,37] Recent studies have shown that activation of AMPK increases the sensitivity of EGFR-TKIs and overcomes the resistance of EGFR mutant lung cancer.[29,38]

In this regard, the effect of coadministration of spirosnuolide B (**2**), with gefitinib was investigated to determine whether it could increase the sensitivity of HCC827 cells to gefitinib. Co-treatment with gefitinib and spirosnuolide B (**2**) exhibited relatively higher antiproliferative activity than treatment with either drug alone (Figures 7 and S16a). The synergistic effect on the induction of apoptosis by cotreatment of spirosnuolide B (**2**) and gefitinib was confirmed by the upregulation of cleaved PARP and downregulation of Bcl-xL expression in

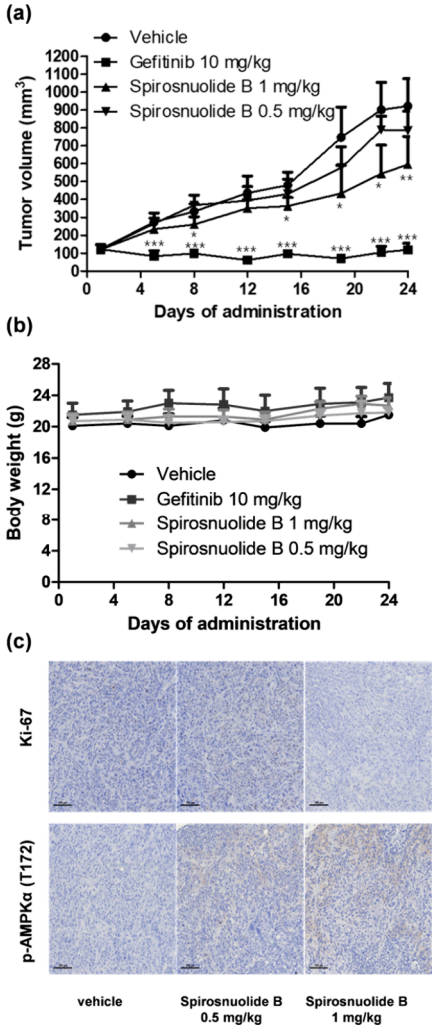

Figure 6. *In vivo* efficacy of spirosnuolide B (**2**). (a) HCC827 cells were implanted subcutaneously into the flank of Balb/C-nude mice. After tumor volume reached approximately 100 mm^3, gefitinib (10 mg/kg) was administered orally or the vehicle and spirosnuolide B (0.5 or 1 mg/kg) was administered intraperitoneally three times per week for 22 days. Tumor volume was measured every 2−3 days. Gefitinib was used as a positive control. *p < 0.05, **p < 0.01, and ***p < 0.001 represent statistically significant differences compared to the vehicle-treated control group. (b) Body weight was monitored twice per week. (c) Excised tumor section was fixed with formalin, embedded in paraffin, incubated with indicated antibodies, and photographed under an inverted phase-contrast microscope.

HCC827 cells, which indicated a potential combinational therapeutic strategy for overcoming gefitinib resistance in EGFR mutant NSCLC (Figure S16b).

CONCLUSION

Spirosnuolides A−D (**1**−**4**), discovered from termite nest-derived *Kitasatospora* sp. INHA29 represent an intriguing array of structural features: (i) The 18-membered macrolides with an embedded [6,6]-spiroketal moiety inside the macrocycle are distinct compared to other bacterial spiroketal-containing macrolides, such as avermectins,[16] oligomycins,[18] ossamycins,[39] or neaumycins[40] because these macrolides bear only one tetrahydropyran ring of the bicyclic spiroketal group in their macrocyclic rings, whereas both tetrahydropyran rings are involved in the macrocycles in **1**−**4**. (ii) Significantly,

https://doi.org/10.1021/jacsau.4c00803
JACS Au 2024, 4, 4821−4832

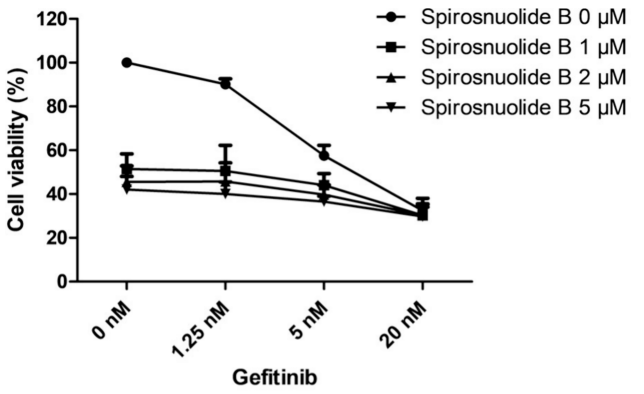

Comp. 2 (μM) / Gefitinib (nM)	1		2		5	
	CI	Description	CI	Description	CI	Description
20	0.51	Synergism	0.57	Synergism	0.68	Synergism
5	0.60	Synergism	0.59	Synergism	0.85	Moderate synergism
1.25	0.89	Slight synergism	0.87	Slight synergism	1.04	Nearly additive

Figure 7. Combination index (CI) value with cotreatment of spirosnuolide B (**2**) and gefitinib in HCC827 cells. Cells were treated with spirosnuolide B (**2**) and gefitinib with indicated concentrations for 48 h, and CI values were calculated for the combination effects.

spirosnuolides were further functionalized with very rare 5- and 6-membered ring-bearing side chains, respectively, adding to the complexity and the novelty of spiroketal macrolides. In particular, the cyclopentenone moiety in spirosnuolide A (**1**) is substituted by multiple functional groups, including hydroxy, methyl, and carboxylic acid, and this combination was previously observed once only in a metabolite isolated from the mangrove endophytic fungus *Alternaria* sp.[41] A database search revealed that the 5-methyl-3,6-dihydroxy-1,4-benzoquinone residue in spirosnuolide B (**2**) has been identified in plants, sponges, mushrooms, and fungi. However, the very recently reported cinnamomycin A is the only one identified from the bacterial world.[11] Hydroxyfuroic acid and butenolide moieties in spirosnuolides C and D have not been previously reported from natural materials, only from bioconversion[19] or synthesis.[42] (iii) The presence of the 1,4-benzoquinone moiety in spirosnuolide B (**2**) exerted significant antiproliferative activity compared to the moieties of the other spirosnuolides, implying the importance of the structural motif. Well-known 1,4-benzoquinone-bearing natural products like oosporein (a symmetrical 1,4-bibenzoquinone derivative from insect pathogenic fungi)[43] and embelin (a lipo-1,4-bibenzoquinone from *Embelia ribes*)[44] have demonstrated cytotoxicity. However, their *in vitro* cytotoxicity against cancer cells is moderate compared with that of spirosnuolide B (**2**). Hence, the antiproliferative activity of spirosnuolide B (**2**) can be attributed to the combination of the spiroketal macrolide core and the 1,4-benzoquinone moiety. (iv) Considering the biosynthetic origin, the spiroketal macrolides in **1**−**4** are biosynthesized by modular type I PKS, whereas cyclopentenone, 1,4-benzoquinone, hydroxyfuroic acid and butenolide originate from type III PKS. Type I/III PKS hybrids are extremely rare in nature. To the best of our knowledge, kendomycins,[15] [7.7]paracyclophanes,[45] venemycins,[46] resorculins,[47] and cinnamomycins[11] are the only compounds claiming to belong to this subclass.

Patients with NSCLC exhibit diverse genetic profiles, with a significant proportion of EGFR overexpression or mutations. Spirosnuolide B (**2**) demonstrated noticeable antiproliferative effects against NSCLC cell lines, with a high safety index. Spirosnuolide B (**2**) activated AMPK, leading to cell cycle arrest and apoptosis in HCC827 cells and inhibited tumor growth. The combination of spirosnuolide B (**2**) and gefitinib exhibited synergistic activity against HCC827 cells, indicating a potential strategy for overcoming gefitinib resistance in EGFR mutant NSCLC. Collectively, spirosnuolide B (**2**) appears to be a promising lead compound, for the discovery of new chemotherapeutic agents for treating NSCLC via activating AMPK signaling.

Type I/III hybrid polyketides have been rarely reported so far, with only several examples documented. Despite their structural uniqueness, the pharmacological evaluation of these hybrid polyketide compounds has been limited to *in vitro* experiments. This study, for the first time, provided that the new type I/III hybrid polyketide, spirosnuolide B (**2**), has great potential as a drug lead based on the mouse model *in vivo* efficacy and its underlying molecular mechanism, indicating the high biomedical value of the untapped and thus yet-to-be-discovered type I/III hybrid polyketides.

METHODS

Detailed information on the compound characterization data, other experimental procedures, copies of 1D and 2D NMR, and HRMS spectra is provided in the Supporting Information.

General Experimental Procedures

Optical rotation values were recorded using a JASCO P-2000 polarimeter (sodium light source, JASCO, Easton, PA, USA) with a 1 cm cell at 25 °C. Ultraviolet (UV) and circular dichroism (CD) spectroscopic data were collected using an Applied Photophysics Chirascan-plus CD spectrometer with a 2 mm CD cell (Applied Photophysics, Leatherhead, Surrey, UK). Infrared (IR) spectra were acquired using a JASCO FT/IR-4200 spectrometer. 1D and 2D NMR spectra were collected using Bruker Avance 500 and 800 MHz (Bruker, Billerica, MA, USA), and JEOL JNM-ECA-600 MHz (JEOL, Tokyo, Japan) spectrometers at the College of Pharmacy, Seoul National University, and Bruker Avance III HD 850 MHz spectrometer (Bruker, Billerica, MA, USA) at the National Center for Inter-University Research Facilities (NCIRF), Seoul National University. Low-resolution electrospray ionization mass spectrometry (LR-ESI-MS) data were obtained using an Agilent Technologies 6130 Quadrupole mass spectrometer interlinked with an Agilent Technologies 1200 series high-performance liquid chromatography (HPLC) instrument (Agilent Technologies, Santa Clara, CA, USA). High-resolution electrospray ionization mass spectrometry (HR-ESI-MS) data were acquired using an AB SCIEX Q-TOF 5600 HR-MS spectrometer (Framingham, MA, USA) at the National Instrumentation Center for Environmental Management (NICEM) at the College of Agriculture and Life Sciences, Seoul National University. The X-ray intensity data were measured on Bruker APEX-III diffractometer equipped with a monochromator with a Mo Kα (λ = 0.71073 Å) incident beam at the National Research Facilities and Equipment Center (NanoBio-Energy Materials Center) in Ewha Womans University.

Purification of Spirosnuolides A−D (1−4, Respectively)

The crude extract was dissolved in methanol (MeOH), adsorbed on 5 g of Celite, loaded on a C_{18} reversed-phase open column (34 × 150 mm), and fractionated sequentially with 500 mL aliquots of 20%, 40%, 60%, 80%, and 100% MeOH in H_2O to yield five fractions. A 15 μL aliquot of each fraction was analyzed by LC/MS, and **1** and **4** were

https://doi.org/10.1021/jacsau.4c00803
JACS Au 2024, 4, 4821−4832

detected in the 80% MeOH−H_2O fraction whereas **2** and **3** were observed from the 100% MeOH fraction.

The 80% MeOH−H_2O fraction was next evaporated and redissolved in MeOH. The sample was then chromatographed with semipreparative reversed-phase HPLC (Kromasil 100−5-C_{18}, 250 × 10 mm, 5 μm) under gradient solvent conditions (60−72% CH_3CN−H_2O with 0.1% formic acid over 24 min; flow rate: 2 mL/min; UV detection: 210 nm) to obtain **1** and **4** at retention times of 19 and 22.5 min, respectively. **1** was further purified using the same HPLC column with isocratic solvent conditions (58% CH_3CN−H_2O with 0.1% formic acid; flow rate: 2 mL/min; UV detection: 210 nm) to yield pure **1** (30 mg) at a retention time of 24 min. **4** was applied on a chiral HPLC column (CHIRALPAK IB, 250 × 4.6 mm, 5 μm) using with isocratic solvent conditions (50% CH_3CN−H_2O with 0.1% formic acid; flow rate: 0.7 mL/min; UV detection: 210 nm) to yield pure **4** at a retention time of 19 min.

To acquire **2** and **3**, the 100% MeOH fraction was also injected into the HPLC column (Kromasil 100−5-C_{18}, 250 × 10 mm, 5 μm) and system mentioned above using a gradient solvent condition (65−85% CH_3CN−H_2O with 0.1% formic acid over 30 min; flow rate: 2 mL/min; UV detection: 210 nm). The procedure was repeated to afford pure form of **2** (45 mg) and **3** (22 mg) at 30 and 24 min, respectively.

Spirosnuolide A (1). white needle crystal; $[\alpha]_D^{20}$ − 44.6 (*c* 0.1, MeOH); UV (MeOH) λ_{max} (log ε) 264 (4.07) nm; IR (neat) ν_{max} 3495, 2975, 2939, 1716, 1362, 1262, 1186, 1155, 1029, 983 cm^{-1}; ^1H and ^{13}C NMR (800 MHz, CD_3OD and acetone-d_6), see Tables S1 and S2; HR-ESI-MS $[M + Na]^+$ *m*/*z* 673.2828 (calcd for $C_{33}H_{46}O_{13}Na^+$, 673.2831), see Figure S131.

Spirosnuolide B (2). yellow block-like crystal; $[\alpha]_D^{20}$ + 113.3 (*c* 0.1, MeOH); UV (CH_3CN) λ_{max} (log ε) 288 (4.82) nm; IR (neat) ν_{max} 3330, 2974, 2944, 1743, 1714, 1641, 1344, 1240, 1187, 1160, 1030, 994 cm^{-1}; ^1H and ^{13}C NMR (500 MHz, CD_3OD and 800 MHz, DMSO-d_6), see Tables S1 and S2; HR-ESI-MS $[M + Na]^+$ *m*/*z* 639.2758 (calcd for $C_{33}H_{44}O_{11}Na^+$, 639.2776), see Figure S132.

Spirosnuolide C (3). white needle crystal; $[\alpha]_D^{20}$ − 64.9 (*c* 0.1, MeOH); UV (MeOH) λ_{max} (log ε) 222 (4.10), 298 (4.17) nm; IR (neat) ν_{max} 3494, 2978, 2938, 1718, 1371, 1242, 1186, 1159, 1030, 989 cm^{-1}; ^1H and ^{13}C NMR (800 MHz, CD_3OD), see Table S1; HR-ESI-MS $[M + Na]^+$ *m*/*z* 655.2706 (calcd for $C_{33}H_{44}O_{12}Na^+$, 655.2725), see Figure S134.

Spirosnuolide D (4). white block-like crystal; $[\alpha]_D^{20}$ − 78.2 (*c* 0.1, MeOH); UV (MeOH) λ_{max} (log ε) 241 (3.80) nm; IR (neat) ν_{max} 3487, 2974, 2930, 1756, 1710, 1608, 1376, 1265, 1193, 1040, 990 cm^{-1}; ^1H and ^{13}C NMR (800 MHz, CD_3OD), see Table S1; HR-ESI-MS $[M + Na]^+$ *m*/*z* 629.2564 (calcd for $C_{31}H_{42}O_{12}Na^+$, 629.2568), see Figure S135.

Genome Sequencing and Analysis

The genome sequencing of the strain *Kitasatospora* sp. INHA29 was performed by CJ Bioscience, Inc. (Seoul, Korea)[48] using the PacBio RS II sequencing platform.[49] The sequencing data was then assembled using Flye (version 2.9),[50] after chimera removal with yacrd (version 0.6.2).[51] Assembled contigs were polished five times using Arrow program. Gene-finding and functional annotation were also performed by CJ Bioscience, Inc. using the EzBioCloud pipeline. In brief, protein-coding sequences (CDSs) were predicted by Prodigal 2.6.2. The CDSs were further annotated with reference to EggNOG 4.5, Swissprot, KEGG, and SEED. A biosynthetic gene cluster (BGC) of spirosnuolides was identified using antiSMASH version 7.0 software. The genome sequence was deposited in GenBank under accession number PP887361. Sequence alignments were performed with Geneious Alignment (alignment type: global alignment (Needleman−Wunsch), global alignment with free end gaps, cost matrix: Blosum 62), and a phylogenetic tree was built with Geneious Tree Builder (Jukes−Cantor, neighbor-joining, and the bootstrap value of 1000 replications) using Geneious Prime 2024.0.3 software (Biomatters Ltd., Auckland, New Zealand).

ASSOCIATED CONTENT

Supporting Information

The Supporting Information is available free of charge at https://pubs.acs.org/doi/10.1021/jacsau.4c00803.

Experimental procedures, compound characterizations, 1D and 2D NMR spectra, HRMS spectra, X-ray data collection, genomic analysis data, and computational studies (PDF)

Crystallographic data (ZIP)

AUTHOR INFORMATION

Corresponding Authors

Sang Kook Lee − *Natural Products Research Institute, College of Pharmacy, Seoul National University, Seoul 08826, Republic of Korea;* orcid.org/0000-0002-4306-7024; Email: sklee61@snu.ac.kr

Dong-Chan Oh − *Natural Products Research Institute, College of Pharmacy, Seoul National University, Seoul 08826, Republic of Korea;* orcid.org/0000-0001-6405-5535; Email: dongchanoh@snu.ac.kr

Authors

Thanh-Hau Huynh − *Natural Products Research Institute, College of Pharmacy, Seoul National University, Seoul 08826, Republic of Korea;* orcid.org/0009-0002-5789-6621

Sung Chul Jang − *Natural Products Research Institute, College of Pharmacy, Seoul National University, Seoul 08826, Republic of Korea*

Yeon Hee Ban − *Department of Molecular Bioscience, College of Biomedical Science, Kangwon National University, Chuncheon 24341, Republic of Korea*

Eun-Young Lee − *Department of Chemistry and Nanoscience, Ewha Womans University, Seoul 03760, Republic of Korea*

Taeho Kim − *Division of Life Science, Department of Bio & Medical Big Data (BK21 Four Program), Research Institute of Life Science, Gyeongsang National University, Jinju 52828, Republic of Korea*

Ilnam Kang − *Department of Biological Sciences, Inha University, Incheon 22212, Republic of Korea*

Joon Soo An − *Natural Products Research Institute, College of Pharmacy, Seoul National University, Seoul 08826, Republic of Korea;* orcid.org/0000-0002-3282-5790

Sangwook Kang − *Natural Products Research Institute, College of Pharmacy, Seoul National University, Seoul 08826, Republic of Korea;* orcid.org/0000-0003-4866-9953

Jaeho Han − *Natural Products Research Institute, College of Pharmacy, Seoul National University, Seoul 08826, Republic of Korea*

Yun Kwon − *Research Institute of Pharmaceutical Science, College of Pharmacy, Kyungpook National University, Daegu 41566, Republic of Korea*

Daehyun Oh − *Research Institute of Pharmaceutical Sciences and College of Pharmacy, Seoul National University, Seoul 08826, Republic of Korea*

Hyeung-geun Park − *Research Institute of Pharmaceutical Sciences and College of Pharmacy, Seoul National University, Seoul 08826, Republic of Korea;* orcid.org/0000-0002-9645-8221

https://doi.org/10.1021/jacsau.4c00803
JACS Au 2024, 4, 4821−4832

Jang-Cheon Cho − *Department of Biological Sciences, Inha University, Incheon 22212, Republic of Korea*
Jichan Jang − *Division of Life Science, Department of Bio & Medical Big Data (BK21 Four Program), Research Institute of Life Science, Gyeongsang National University, Jinju 52828, Republic of Korea*
Ki-Bong Oh − *Department of Agricultural Biotechnology, College of Agriculture and Life Sciences and Natural Products Research Institute, Seoul National University, Seoul 08826, Republic of Korea*
Sang-Jip Nam − *Department of Chemistry and Nanoscience, Ewha Womans University, Seoul 03760, Republic of Korea;* orcid.org/0000-0002-0944-6565

Complete contact information is available at: https://pubs.acs.org/10.1021/jacsau.4c00803

Author Contributions

[¶]Thanh-Hau Huynh and Sung Chul Jang equally contributed to this work. All authors have given approval to the final version of the manuscript.

Funding

This work was supported by the National Research Foundation of Korea grants funded by the Republic of Korean Government (Ministry of Science and ICT) (2020R1A2C2003518, 2021R1A4A2001251, 2022R1A2C3005459, and RS-2024−00352229).

Notes

The authors declare the following competing financial interest(s): The authors submitted patent applications for spirosnuolides and their anticancer activity (10-2024-0022679 and PCT/KR2024/002539).

■ ACKNOWLEDGMENTS

The authors thank Dr. Youngmee Kim for providing the X-ray crystallographic data.

■ REFERENCES

(1) Bray, F.; Laversanne, M.; Sung, H.; Ferlay, J.; Siegel, R. L.; Soerjomataram, I.; Jemal, A. Global Cancer Statistics 2022: GLOBOCAN Estimates of Incidence and Mortality Worldwide for 36 Cancers in 185 Countries. *CA. Cancer J. Clin.* **2024**, *74* (3), 229−263.
(2) Pikor, L. A.; Ramnarine, V. R.; Lam, S.; Lam, W. L. Genetic Alterations Defining NSCLC Subtypes and Their Therapeutic Implications. *Lung Cancer* **2013**, *82* (2), 179−189.
(3) Miller, K. D.; Nogueira, L.; Devasia, T.; Mariotto, A. B.; Yabroff, K. R.; Jemal, A.; Kramer, J.; Siegel, R. L. Cancer Treatment and Survivorship Statistics, 2022. *CA. Cancer J. Clin.* **2022**, *72* (5), 409−436.
(4) Li, Y.; Yan, B.; He, S. Advances and Challenges in the Treatment of Lung Cancer. *Biomed. Pharmacother.* **2023**, *169*, No. 115891.
(5) Williamson, R. T.; Buevich, A. V.; Martin, G. E.; Parella, T. LR-HSQMBC: A Sensitive NMR Technique to Probe Very Long-Range Heteronuclear Coupling Pathways. *J. Org. Chem.* **2014**, *79* (9), 3887−3894.
(6) Williams, P. G.; Asolkar, R. N.; Kondratyuk, T.; Pezzuto, J. M.; Jensen, P. R.; Fenical, W. Saliniketals A and B, Bicyclic Polyketides from the Marine Actinomycete *Salinispora arenicola*. *J. Nat. Prod.* **2007**, *70* (1), 83−88.
(7) Shin, Y.-H.; Beom, J. Y.; Chung, B.; Shin, Y.; Byun, W. S.; Moon, K.; Bae, M.; Lee, S. K.; Oh, K.-B.; Shin, J.; Yoon, Y. J.; Oh, D.-C. Bombyxamycins A and B, Cytotoxic Macrocyclic Lactams from an Intestinal Bacterium of the Silkworm *Bombyx mori*. *Org. Lett.* **2019**, *21* (6), 1804−1808.
(8) Joseph-Nathan, P.; Abramo-Bruno, D.; Ortega, D. A. Carbon-13 NMR Studies of Benzoquinones. *Org. Magn. Reson.* **1981**, *15* (3), 311−316.
(9) Kubo, I.; Chaudhuri, S. K. Structure of Maesaquinone. *Bioorg. Med. Chem. Lett.* **1994**, *4* (9), 1131−1134.
(10) Danquah, M. Embelin and Its Derivatives: Design, Synthesis, and Potential Delivery Systems for Cancer Therapy. *Pharmaceuticals* **2022**, *15* (9), 1131.
(11) Zhang, B.; Jin, W.; Zhang, Y.; Dai, Y.; Li, H.; Sun, Y.; Wu, X.; Luo, J.; Chen, Y. A Type I/Type III PKS Hybrid Generates Cinnamomycin A−D. *Org. Lett.* **2023**, *25* (15), 2560−2564.
(12) Burgueño-Tapia, E.; Joseph-Nathan, P. ^{13}C NMR Substituent Chemical Shifts in Hydroxy-*p*-Benzoquinones. *Magn. Reson. Chem.* **2000**, *38* (5), 390−393.
(13) Blin, K.; Shaw, S.; Augustijn, H. E.; Reitz, Z. L.; Biermann, F.; Alanjary, M.; Fetter, A.; Terlouw, B. R.; Metcalf, W. W.; Helfrich, E. J. N.; van Wezel, G. P.; Medema, M. H.; Weber, T. antiSMASH 7.0: New and Improved Predictions for Detection, Regulation, Chemical Structures and Visualisation. *Nucleic Acids Res.* **2023**, *51* (W1), W46−W50.
(14) Wenzel, S. C.; Bode, H. B.; Kochems, I.; Müller, R. A Type I/Type III Polyketide Synthase Hybrid Biosynthetic Pathway for the Structurally Unique Ansa Compound Kendomycin. *ChemBioChem.* **2008**, *9* (16), 2711−2721.
(15) Chen, J.; Zhang, S.; Chen, Y.; Tian, X.; Gu, Y.; Ju, J. Identification and Heterologous Expression of the Kendomycin B Biosynthetic Gene Cluster from *Verrucosispora* sp. SCSIO 07399. *Mar. Drugs* **2021**, *19* (12), 673.
(16) Sun, P.; Zhao, Q.; Yu, F.; Zhang, H.; Wu, Z.; Wang, Y.; Wang, Y.; Zhang, Q.; Liu, W. Spiroketal Formation and Modification in Avermectin Biosynthesis Involves a Dual Activity of AveC. *J. Am. Chem. Soc.* **2013**, *135* (4), 1540−1548.
(17) Takahashi, S.; Toyoda, A.; Sekiyama, Y.; Takagi, H.; Nogawa, T.; Uramoto, M.; Suzuki, R.; Koshino, H.; Kumano, T.; Panthee, S.; Dairi, T.; Ishikawa, J.; Ikeda, H.; Sakaki, Y.; Osada, H. Reveromycin A Biosynthesis Uses RevG and RevJ for Stereospecific Spiroacetal Formation. *Nat. Chem. Biol.* **2011**, *7* (7), 461−468.
(18) Bilyk, O.; Oliveira, G. S.; de Angelo, R. M.; Almeida, M. O.; Honório, K. M.; Leeper, F. J.; Dias, M. V. B.; Leadlay, P. F. Enzyme-Catalyzed Spiroacetal Formation in Polyketide Antibiotic Biosynthesis. *J. Am. Chem. Soc.* **2022**, *144* (32), 14555−14563.
(19) Chen, S.-S. T.; Zhang, B. B.; Li, X. Antidiabetic 4-Hydroxy-2-Furoic Acids. US 2003/0134890 A1, 2003.
(20) Long, Y. C.; Zierath, J. R. AMP-Activated Protein Kinase Signaling in Metabolic Regulation. *J. Clin. Invest.* **2006**, *116* (7), 1776−1783.
(21) Choi, Y. K.; Park, K.-G. Metabolic Roles of AMPK and Metformin in Cancer Cells. *Mol. Cells* **2013**, *36* (4), 279−287.
(22) Kim, I.; He, Y.-Y. Targeting the AMP-Activated Protein Kinase for Cancer Prevention and Therapy. *Front. Oncol.* **2013**, *3*, 175.
(23) Xia, Y.; Zha, J.; Sang, Y.-H.; Yin, H.; Xu, G.; Zhen, J.; Zhang, Y.; Yu, B. AMPK Activation by ASP4132 Inhibits Non-Small Cell Lung Cancer Cell Growth. *Cell Death Dis.* **2021**, *12* (4), 365.
(24) Villanueva-Paz, M.; Cotán, D.; Garrido-Maraver, J.; Oropesa-Ávila, M.; de la Mata, M.; Delgado-Pavón, A.; de Lavera, I.; Alcocer-Gómez, E.; Álvarez-Córdoba, M.; Sánchez-Alcázar, J. A. AMPK Regulation of Cell Growth, Apoptosis, Autophagy, and Bioenergetics. In *AMP-activated Protein Kinase*; Cordero, M. D., Viollet, B., Eds.; Springer International Publishing: Cham, 2016; pp 45−71. DOI: DOI: 10.1007/978-3-319-43589-3_3.
(25) Shao, J.; Zhang, A.; Qin, W.; Zheng, L.; Zhu, Y.; Chen, X. AMP-Activated Protein Kinase (AMPK) Activation Is Involved in Chrysin-Induced Growth Inhibition and Apoptosis in Cultured A549 Lung Cancer Cells. *Biochem. Biophys. Res. Commun.* **2012**, *423* (3), 448−453.
(26) Kang, J. I.; Hong, J.-Y.; Lee, H.-J.; Bae, S. Y.; Jung, C.; Park, H. J.; Lee, S. K. Anti-Tumor Activity of Yuanhuacine by Regulating

AMPK/mTOR Signaling Pathway and Actin Cytoskeleton Organization in Non-Small Cell Lung Cancer Cells. *PLoS One* **2015**, *10* (12), No. e0144368.
(27) Wei, C.; Yao, X.; Jiang, Z.; Wang, Y.; Zhang, D.; Chen, X.; Fan, X.; Xie, C.; Cheng, J.; Fu, J.; Leung, E. L.-H. Cordycepin Inhibits Drug-Resistance Non-Small Cell Lung Cancer Progression by Activating AMPK Signaling Pathway. *Pharmacol. Res.* **2019**, *144*, 79−89.
(28) Hülsmann, H. J.; Rolff, J.; Bender, C.; Jarahian, M.; Korf, U.; Herwig, R.; Fröhlich, H.; Thomas, M.; Merk, J.; Fichtner, I.; Sültmann, H.; Kuner, R. Activation of AMP-Activated Protein Kinase Sensitizes Lung Cancer Cells and H1299 Xenografts to Erlotinib. *Lung Cancer* **2014**, *86* (2), 151−157.
(29) Li, L.; Wang, T.; Hu, M.; Zhang, Y.; Chen, H.; Xu, L. Metformin Overcomes Acquired Resistance to EGFR TKIs in EGFR-Mutant Lung Cancer via AMPK/ERK/NF-κB Signaling Pathway. *Front. Oncol.* **2020**, *10*, 1605.
(30) Witters, L. A.; Nordlund, A.-C.; Marshall, L. Regulation of Intracellular Acetyl-CoA Carboxylase by ATP Depletors Mimics the Action of the 5′-AMP-Activated Protein Kinase. *Biochem. Biophys. Res. Commun.* **1991**, *181* (3), 1486−1492.
(31) Egan, D. F.; Shackelford, D. B.; Mihaylova, M. M.; Gelino, S.; Kohnz, R. A.; Mair, W.; Vasquez, D. S.; Joshi, A.; Gwinn, D. M.; Taylor, R.; Asara, J. M.; Fitzpatrick, J.; Dillin, A.; Viollet, B.; Kundu, M.; Hansen, M.; Shaw, R. J. Phosphorylation of ULK1 (hATG1) by AMP-Activated Protein Kinase Connects Energy Sensing to Mitophagy. *Science* **2011**, *331* (6016), 456−461.
(32) Zoncu, R.; Efeyan, A.; Sabatini, D. M. mTOR: From Growth Signal Integration to Cancer, Diabetes and Ageing. *Nat. Rev. Mol. Cell Biol.* **2011**, *12* (1), 21−35.
(33) Matthews, H. K.; Bertoli, C.; de Bruin, R. A. M. Cell Cycle Control in Cancer. *Nat. Rev. Mol. Cell Biol.* **2022**, *23* (1), 74−88.
(34) Milletti, G.; Colicchia, V.; Cecconi, F. Cyclers' Kinases in Cell Division: From Molecules to Cancer Therapy. *Cell Death Differ.* **2023**, *30* (9), 2035−2052.
(35) Otto, T.; Sicinski, P. Cell Cycle Proteins as Promising Targets in Cancer Therapy. *Nat. Rev. Cancer* **2017**, *17* (2), 93−115.
(36) Giaccone, G.; Herbst, R. S.; Manegold, C.; Scagliotti, G.; Rosell, R.; Miller, V.; Natale, R. B.; Schiller, J. H.; von Pawel, J.; Pluzanska, A.; Gatzemeier, U.; Grous, J.; Ochs, J. S.; Averbuch, S. D.; Wolf, M. K.; Rennie, P.; Fandi, A.; Johnson, D. H. Gefitinib in Combination With Gemcitabine and Cisplatin in Advanced Non−Small-Cell Lung Cancer: A Phase III Trial—INTACT 1. *J. Clin. Oncol.* **2004**, *22* (5), 777−784.
(37) Herbst, R. S.; Giaccone, G.; Schiller, J. H.; Natale, R. B.; Miller, V.; Manegold, C.; Scagliotti, G.; Rosell, R.; Oliff, I.; Reeves, J. A.; Wolf, M. K.; Krebs, A. D.; Averbuch, S. D.; Ochs, J. S.; Grous, J.; Fandi, A.; Johnson, D. H. Gefitinib in Combination With Paclitaxel and Carboplatin in Advanced Non−Small-Cell Lung Cancer: A Phase III Trial—INTACT 2. *J. Clin. Oncol.* **2004**, *22* (5), 785−794.
(38) Kim, S. M.; Yun, M. R.; Hong, Y. K.; Solca, F.; Kim, J.-H.; Kim, H.-J.; Cho, B. C. Glycolysis Inhibition Sensitizes Non−Small Cell Lung Cancer with T790M Mutation to Irreversible EGFR Inhibitors via Translational Suppression of Mcl-1 by AMPK Activation. *Mol. Cancer Ther.* **2013**, *12* (10), 2145−2156.
(39) Bilyk, O.; Samborskyy, M.; Leadlay, P. F. The Biosynthetic Pathway to Ossamycin, a Macrocyclic Polyketide Bearing a Spiroacetal Moiety. *PLoS One* **2019**, *14* (4), No. e0215958.
(40) Kim, M. C.; Machado, H.; Jang, K. H.; Trzoss, L.; Jensen, P. R.; Fenical, W. Integration of Genomic Data with NMR Analysis Enables Assignment of the Full Stereostructure of Neaumycin B, a Potent Inhibitor of Glioblastoma from a Marine-Derived *Micromonospora*. *J. Am. Chem. Soc.* **2018**, *140* (34), 10775−10784.
(41) Wang, J.; Ding, W.; Wang, R.; Du, Y.; Liu, H.; Kong, X.; Li, C. Identification and Bioactivity of Compounds from the Mangrove Endophytic Fungus *Alternaria* sp. *Mar. Drugs* **2015**, *13* (7), 4492−4504.
(42) Evanno, L.; Lachkar, D.; Lamali, A.; Boufridi, A.; Séon-Méniel, B.; Tintillier, F.; Saulnier, D.; Denis, S.; Genta-Jouve, G.; Jullian, J.-C.; Leblanc, K.; Beniddir, M. A.; Petek, S.; Debitus, C.; Poupon, E. A Ring-Distortion Strategy from Marine Natural Product Ilimaquinone Leads to Quorum Sensing Modulators. *Eur. J. Org. Chem.* **2018**, *2018* (20−21), 2486−2497.
(43) Ramesha, A.; Venkataramana, M.; Nirmaladevi, D.; Gupta, V. K.; Chandranayaka, S.; Srinivas, C. Cytotoxic Effects of Oosporein Isolated from Endophytic Fungus *Cochliobolus kusanoi*. *Front. Microbiol.* **2015**, *6*, 870.
(44) Ko, J.-H.; Lee, S.-G.; Yang, W. M.; Um, J.-Y.; Sethi, G.; Mishra, S.; Shanmugam, M. K.; Ahn, K. S. The Application of Embelin for Cancer Prevention and Therapy. *Molecules* **2018**, *23* (3), 621.
(45) Larsen, J. S.; Pearson, L. A.; Neilan, B. A. Genome Mining and Evolutionary Analysis Reveal Diverse Type III Polyketide Synthase Pathways in Cyanobacteria. *Genome Biol. Evol.* **2021**, *13* (4), No. evab056.
(46) Thanapipatsiri, A.; Gomez-Escribano, J. P.; Song, L.; Bibb, M. J.; Al-Bassam, M.; Chandra, G.; Thamchaipenet, A.; Challis, G. L.; Bibb, M. J. Discovery of Unusual Biaryl Polyketides by Activation of a Silent *Streptomyces venezuelae* Biosynthetic Gene Cluster. *ChemBioChem* **2016**, *17* (22), 2189−2198.
(47) Lacey, H. J.; Chen, R.; Vuong, D.; Lacey, E.; Rutledge, P. J.; Chooi, Y.-H.; Piggott, A. M.; Booth, T. J. Resorculins: Hybrid Polyketide Macrolides from *Streptomyces* sp. MST-91080. *Org. Biomol. Chem.* **2023**, *21* (12), 2531−2538.
(48) Yoon, S.-H.; Ha, S.-M.; Kwon, S.; Lim, J.; Kim, Y.; Seo, H.; Chun, J. Introducing EzBioCloud: A Taxonomically United Database of 16S rRNA Gene Sequences and Whole-Genome Assemblies. *Int. J. Syst. Evol. Microbiol.* **2017**, *67*, 1613−1617.
(49) Rhoads, A.; Au, K. F. PacBio Sequencing and Its Applications. *SI Metagenomics Mar. Environ.* **2015**, *13* (5), 278−289.
(50) Kolmogorov, M.; Yuan, J.; Lin, Y.; Pevzner, P. A. Assembly of Long, Error-Prone Reads Using Repeat Graphs. *Nat. Biotechnol.* **2019**, *37* (5), 540−546.
(51) Marijon, P.; Chikhi, R.; Varré, J.-S. Yacrd and Fpa: Upstream Tools for Long-Read Genome Assembly. *Bioinformatics* **2020**, *36* (12), 3894−3896.

https://doi.org/10.1021/jacsau.4c00803
JACS Au 2024, 4, 4821−4832